

Multi-generation Chemical Aging of α -Pinene Ozonolysis Products by Reactions with OH

N. Wang¹, E. Kostenidou^{2,3}, N. M. Donahue¹ and S. N. Pandis^{1,2,3}

¹Department of Chemical Engineering, Carnegie Mellon University, Pittsburgh, US

²Department of Chemical Engineering, University of Patras, Patra, Greece

³Institute of Chemical Engineering Sciences (ICE-HT), FORTH, Patra, Greece

Abstract

Secondary organic aerosol (SOA) formation from volatile organic compounds (VOCs) in the atmosphere can be thought of as a succession of oxidation steps. The production of later-generation SOA via continued oxidation of the first-generation products is defined as chemical aging. This study investigates aging in the α -pinene ozonolysis system with hydroxyl radicals (OH) through smog chamber experiments. The first-generation α -pinene ozonolysis products were allowed to react further with OH formed via HONO photolysis. After an equivalent of 2-4 days of typical atmospheric oxidation conditions, homogeneous OH oxidation of the α -pinene ozonolysis products resulted in a 20-40 % net increase of the SOA for the experimental conditions used in this work. A more oxygenated product distribution was observed after aging based on the increase in aerosol atomic oxygen to carbon ratio (O:C) by up to 0.04. Experiments performed at intermediate relative humidity (RH) of 50 % showed no significant difference in additional SOA formation during aging compared to those performed at low RH of less than 20 %.

1. Introduction

Anthropogenic activities such as fuel combustion as well as biogenic sources such as emissions from vegetation can introduce particles and particle precursors into the atmosphere. In most areas, about half of the submicron aerosol mass on average is composed of organic compounds (Zhang et al., 2007). Organic particles directly emitted to the atmosphere are traditionally defined as primary organic aerosol (POA), while those formed through atmospheric

29 reactions and condensation of species with corresponding volatility are secondary (SOA).
30 Atmospheric aerosols represent a significant risk to human health by causing respiratory problems
31 and heart attacks (Davidson et al., 2005; Pope et al., 2009). At the same time these particles
32 influence the climate of our planet (Intergovernmental Panel on Climate Change, 2007).

33 Oxygenated OA with a high oxygen to carbon ratio (O:C) is often the most important
34 component of ambient OA suggesting the importance of atmospheric chemistry in the formation
35 and processing of OA (Zhang et al., 2007). Early studies of SOA formation focused on the first
36 stage of reactions involving the target precursor reacting with the chosen oxidant. In the
37 atmosphere, organic vapors and particles interact with oxidants for days and therefore successive
38 oxidation processes are inevitable.

39 Chemical aging refers to the subsequent stages of SOA formation and evolution due to the
40 production of later-generation products via oxidation of first-generation products by oxidants such
41 as OH free radicals (Donahue et al., 2006; Henry et al., 2012). Previous studies have explored
42 various forms of aging, including heterogeneous reactions of oxidants and aerosols (George et al.,
43 2008), oligomerization (Kalberer et al., 2006), photolysis of either gas or condensed-phase
44 products (Henry and Donahue, 2012), and homogeneous gas-phase oxidation by OH (Donahue et
45 al., 2012). Homogeneous gas-phase oxidation reactions appear to be in general much faster than
46 heterogeneous reactions, due to diffusion limitations of the latter (Lambe et al., 2009). The first-
47 generation oxidation reactions of most SOA precursors convert much less than 50 % of the
48 precursor to SOA, leaving more than half of the carbon still in the gas-phase. Additional oxidation
49 of these vapors can potentially contribute additional and more oxygenated SOA components.
50 These later-generation reactions have been proposed to be a major missing step connecting
51 chamber studies to field measurements.

52 Zeroth order parameterizations have been developed to model the chemical aging of semi-
53 volatile POA emissions in chemical transport models (Robinson et al., 2007). CTMs using these
54 schemes show improved performance in urban areas such as Mexico City (Tsimpidi et al., 2011),
55 but tend to over-predict OA in areas such as the southeastern United States where biogenic VOCs
56 dominate if chemical aging is assumed to be a major source of additional SOA (Lane et al., 2008).
57 As a result, the importance of aging of biogenic SOA as a source of SOA mass concentration
58 remains an issue of debate.

59 The ozonolysis of α -pinene ($C_{10}H_{16}$) is considered one of the most important global SOA
60 sources (Griffin et al., 1999). The system has been well characterized through smog chamber
61 experiments where researchers quantified its SOA yields under different conditions, explored the
62 reaction pathways and mechanisms, and identified its product distributions. Recent studies suggest
63 that there is significant potential for additional SOA formation from homogeneous gas-phase aging
64 by OH of the first-generation α -pinene oxidation products (Donahue et al., 2012; Müller et al.,
65 2012; Chacon-Madrid et al., 2013). Major identified products existing in gas phase such as
66 pinonaldehyde and pinonic acid can serve as SOA precursors and further react with OH.
67 Pinonaldehyde reacts with OH, with SOA mass yields up to 5 % under low- NO_x conditions and
68 20 % under high- NO_x conditions (Chacon-Madrid et al., 2013). Müller et al. (2012) demonstrated
69 the formation of 1,2,3-butanetricarboxylic acid (MBTCA), an SOA product of low volatility
70 identified in α -pinene ozonolysis, through the gas-phase OH oxidation of pinonic acid. They
71 reported an experimental yield of 0.6 % for MBTCA from the gas-phase OH oxidation of pinonic
72 acid, accounting for about 10 % of the total SOA formed. The proposed formation mechanisms of
73 MBTCA is a classic example of semi-volatile precursors going through oxidation and forming
74 products of lower volatility.

75 The Multiple Chamber Aerosol Chemical Aging Study (MUCHACHAS) explored the gas-
76 phase OH aging effects of the α -pinene ozonolysis products via experiments performed in four
77 different smog chambers (Donahue et al., 2012). They were able to isolate the aging effect by
78 using different OH sources (HOOH photolysis, HONO photolysis, TME ozonolysis), light sources
79 (sunlight, quasi-solar lamps, 350 nm UV lamps), and chambers of different design in size and
80 material (Teflon and aluminum). Almost in all experiments, additional formation of SOA (up to
81 55 %) and a more oxidized product distribution (increasing O:C) were observed after aging.
82 However, in one of the chambers, strong UV photolysis led to decreasing SOA mass
83 concentrations in experiments with low to moderate OH levels, $[OH] \leq 2 \times 10^6$ molecules cm^{-3}
84 (Henry and Donahue, 2012). These authors concluded that chemical aging involves a complex set
85 of interacting processes with competing functionalization (conserved C number with products of
86 lower volatility and higher oxidation states) and fragmentation (cleavage of C-bond with products
87 over a wide volatility range and higher oxidation states) of the various organic compounds. A 2D-
88 volatility basis set (2D-VBS) simulation based on these two pathways and a branching ratio
89 between them showed that homogeneous OH aging can potentially more than double the α -pinene

90 SOA mass concentration, after about a day's equivalent of typical atmospheric oxidation
91 conditions. Uncertainties such as "ripening" during which SOA volatility evolves but its mass
92 remains constant, UV photolysis and heterogeneous OH uptake can further complicate the aging
93 process.

94 Qi et al. (2012) also explored aging of the α -pinene ozonolysis system through smog
95 chamber experiments using HOOH as an OH source and studied the UV photolysis effect. They
96 observed a 7.5 % increase in the SOA volume concentration and an increase of 0.03 in the O:C
97 after aging. Minimum photolysis effect was reported for these experiments.

98 One complication of chamber experiments is the interaction of particles with chamber
99 walls. The wall-loss rate of particles is a function of particle size, charge distribution, chamber
100 geometry, turbulence, and electric field within the chamber (Crump and Seinfeld, 1981). In order
101 to quantify SOA yields from chamber experiments, it is important to correct for particle wall loss.
102 Recent findings that organic vapors in the chamber can be directly lost to the Teflon walls as well
103 further complicate the wall-loss correction process (Matsunaga and Ziemann, 2010; Zhang et al.,
104 2014). Krechmer et al. (2016) measured the loss rate of vapors formed in the chamber and found
105 the corresponding timescale to be 7-13 min. Ye et al. (2016) determined the vapor wall-loss
106 timescale in the Carnegie Mellon chamber used in this work to be around 15 min for semi-volatile
107 organic compounds.

108 Despite the consensus from the aforementioned chamber studies that gas-phase OH aging
109 of α -pinene ozonolysis products can contribute to additional SOA formation, there lacks
110 consistency in the extent to which the additional mass can form for different OH exposures. Part
111 of the problem is that the estimated amount of additional SOA formed from these long-lasting
112 aging experiments can be extra sensitive to the particle and the vapor wall-loss correction methods
113 deployed. The uncertainties at the end of a 10-hour long aging experiment during which most
114 particles are lost to chamber walls and the measured suspended mass is low can be relatively high.
115 In this work, we aim to quantify the additional SOA formed during the aging step comparing
116 measurements from a suite of instrumentation. We adopt a size-dependent particle wall-loss
117 correction method and develop a procedure to better constrain the associated errors. We also
118 attempt to constrain the vapor loss using both theoretical calculations and measurements.

119

120

121 2. Experimental approach

122 We conducted experiments in a 12 m³ Teflon (Welch Fluorocarbons) smog chamber at
123 Carnegie Mellon University (CMU). The reactor was suspended in a temperature-controlled room
124 with walls covered with UV lights (GE 10526 and 10244). Prior to each experiment, we flushed
125 the chamber overnight with purified air under UV illumination to remove any residual particles
126 and gas-phase organics. We generated purified air by passing ambient air through a high-efficiency
127 particulate air (HEPA) filter to remove particles, an activated carbon filter to remove any organics,
128 a Purafil filter to remove NO_x, and finally a silica gel filter, keeping relative humidity (RH) below
129 5 % in the chamber before each experiment.

130 We pumped an ammonium sulfate solution (1 g L⁻¹) into the chamber at the beginning of
131 each experiment through an atomizer (TSI, model 3076) at a constant rate of 90 mL h⁻¹ to produce
132 droplets. The droplets passed through a diffusion dryer and a neutralizer to produce dry ammonium
133 sulfate seed particles. We injected seeds with a number mode size of 110 nm until they reached a
134 number concentration of 2×10⁴ cm⁻³, resulting in an initial seed mass concentration of around 40
135 μg m⁻³ and a surface area concentration of up to 1000 μm² cm⁻³. Typical organic vapors with a
136 molar weight of 250 g mol⁻¹ thus had an initial collision frequency with these seeds of 0.01 s⁻¹. We
137 injected α-pinene (Sigma-Aldrich, ≥ 99 %) into the chamber using a septum injector with purified
138 air as carrier flow. We generated ozone using a corona-discharge ozone generator (AZCO,
139 HTU500AC) to initiate the ozonolysis reaction. We prepared a fresh HONO solution in a bubbler
140 by adding a 4.9 g L⁻¹ sulfuric acid solution to a 6.9 g L⁻¹ sodium nitrite solution. We then turned
141 on the UV lights to start the photo-dissociation of HONO, producing OH.

142 At the end of each experiment, we injected additional ammonium-sulfate seeds into the
143 chamber using the same method with a more concentrated solution (5 g L⁻¹) in order to characterize
144 the particle wall-loss rates a second time.

145 We added butanol-d9 (Cambridge Isotope Laboratories, 98 %) into the chamber through
146 the septum injector as an OH tracer before the reaction started and used the method described in
147 Barmet et al. (2012) to calculate the OH produced by HONO photolysis. The OH concentration in
148 these experiments was around 2.4×10⁷ molecules cm⁻³ for the first hour, then dropped to around
149 5×10⁶ molecules cm⁻³ afterwards. The introduction and photolysis of HONO produces hundreds
150 of ppb of NO_x, and thus the aging reactions in this work occurred under high NO_x conditions; the
151 majority of the peroxy radicals reacted with NO during the aging phase of the experiments.

152 We performed experiments at both low RH of less than 20 % and intermediate RH of 50 %.
153 To add water vapor to the chamber, we used a stream of purified air to carry ultrapure water
154 (Millipore water purification system) in a bubbler into the chamber before the introduction of seeds.

155 We measured the particle size distribution using a TSI Scanning Mobility Particle Sizer,
156 SMPS (classifier model 3080; CPC model 3010 or 3772), with flows adjusted to measure particle
157 diameters in the 15-700 nm range. We measured the particle composition and mass spectrum of
158 the OA with an Aerodyne High Resolution Time-of-flight Aerosol Mass Spectrometer (HR-ToF-
159 AMS). We monitored the concentrations of α -pinene and butanol-d9 using a Proton Transfer
160 Reaction-Mass Spectrometer (PTR-MS, Ionicon), the ozone concentration using a Dasibi 1008
161 ozone monitor (ICE: Teledyne 400E), and NO_x ($\text{NO} + \text{NO}_2$) levels using a Teledyne API NO_x
162 Analyzer 200A (ICE: Teledyne T201). We held the chamber temperature constant at 22 °C
163 throughout all experiments. We list the initial conditions of the experiments performed for this
164 work in Table 1.

165

166 **3. Data analysis**

167 **3.1 SOA yields**

168 The SOA mass yield, Y , is a metric of the ability of a gaseous precursor to form SOA, and
169 is defined as $Y = C_{\text{SOA}}/\Delta\text{VOC}$, where C_{SOA} is the produced SOA mass concentration (in $\mu\text{g m}^{-3}$)
170 and ΔVOC the amount of the VOC precursor (α -pinene in this case) reacted (in $\mu\text{g m}^{-3}$). To
171 separate the effect of aging on SOA mass concentration, we define a first-generation SOA mass
172 yield, $Y_1 = C_{\text{SOA},1}/\Delta\text{VOC}$, and a second-generation SOA mass yield, $Y_2 = C_{\text{SOA},2}/\Delta\text{VOC}$. $C_{\text{SOA},1}$ and
173 $C_{\text{SOA},2}$ are the concentrations of SOA formed before, and after aging with hydroxyl radicals. All
174 α -pinene reacts away during the first stage and thus ΔVOC for the second stage is the same as the
175 initial α -pinene concentration in the chamber.

176

177 **3.2 Particle wall-loss correction**

178 In this work, we try to reduce the uncertainties in the estimated SOA mass concentration
179 associated with the particle wall-loss correction. This uncertainty can be significant due to two
180 aspects of these aging experiments: the evolution of the particle size distribution and the duration
181 of the experiments. In these aging experiments, where particles grow by condensation and
182 coagulation for several hours, the particle size distribution can potentially shift, covering a wide

183 size range over the course of an experiment. Particle wall losses are size dependent, and this shift
184 can introduce significant errors if a constant loss rate constant is assumed. To minimize these
185 problems, we adopted a size-dependent particle wall-loss correction method where we determined
186 the particle wall-loss rate constant, k , at each particle size, D_p .

187

188 **3.2.1 Determination of particle wall-loss rate constants**

189 The size-dependent particle wall-loss correction method (Keywood et al., 2004; Ng et al.,
190 2007; Loza et al., 2012; Nah et al., 2016) adopted in this work is based on the SMPS-measured
191 particle size distribution. At each particle size bin i , the first-order particle wall-loss rate constant
192 k , can be determined as the slope of the following equation:

193

$$194 \ln[N_i(t)] = -k_i t + Q \quad (1)$$

195

196 where $N_i(t)$ is the SMPS-measured aerosol number concentration at size bin i and Q is an arbitrary
197 constant. Applying Eqn. 1 across the entire SMPS-measured particle size range, we obtain the
198 particle wall-loss rate constant function, $k(D_p)$.

199 To determine the $k(D_p)$ profile, we utilized the initial four-hour ammonium sulfate seed
200 wall-loss period for each experiment. Since k may also vary with time (McMurry and Rader, 1985),
201 we determined a second $k(D_p)$ profile for each experiment using the ammonium sulfate seed wall-
202 loss period at the end. It is important to ensure that the k 's, especially at sizes where the majority
203 of SOA mass is distributed, remain the same over the course of each experiment.

204 The $k(D_p)$ values calculated (with an $R^2 > 0.5$) based on SMPS measurements of the seed
205 distribution from this work usually only cover particle size range of 30-300 nm due to the lack of
206 particles at either end of the particle size distribution. To determine the $k(D_p)$ for $D_p < 30$ nm, we
207 use a simple log-linear fit of k 's from 30-50 nm and back extrapolate it to 10 nm. To determine
208 $k(D_p)$ for $D_p > 300$ nm, we assume that the constant is practically the same in the 300-700 nm
209 range. We confirmed this with additional seed-only experiments where there were enough particles
210 at that size range (Wang et al., 2017). Significant increases of the rate loss constant are observed
211 for particles larger than 1 μm , while in our experiments the particles remained small than 600 nm
212 or so. A measure of the uncertainty of these corrections is the variability of the corrected mass
213 concentration during the seed wall-loss periods as discussed in the next section. Details regarding

214 the wall-loss profiles in the CMU chamber and the execution of the size-dependent particle wall-
 215 loss correction for this work can be found in Wang et al. (2017).

216

217 3.2.2 Correction of SMPS measurements

218 The corrected particle number concentration at each size bin i , $N_i(t)$, can be calculated
 219 numerically,

220

$$221 N_i(t) = N_i^m(t) + k_i \int_0^t N_i^m(t) dt, \quad (2)$$

222

223 from the measured values $N_i^m(t)$ and the $k(D_p)$ corresponding to the size bin i , k_i .

224 For closed systems in which coagulation is slow, the particle wall-loss corrected number
 225 concentration should be constant. In order to evaluate how well the correction works, we define
 226 the parameter: $\varepsilon_N = 2\sigma_{N_s}/\overline{N_s}$, where σ_{N_s} is the standard deviation of the particle wall-loss
 227 corrected number concentration for the seed wall-loss periods and $\overline{N_s}$ the average. Similarly, we
 228 define $\varepsilon_V = 2\sigma_{N_s}/\overline{V_s}$ based on the particle wall-loss corrected volume concentration for the two
 229 seed wall-loss periods. Only when all four values, ε_N and ε_V for both the initial and the final seed
 230 periods, are less than 5 % do we deem the particle wall-loss correction valid for that individual
 231 experiment. Experiments in which these criteria were not met were not included in the analysis.

232 To calculate the mass concentration of the formed SOA, C_{SOA} , during the course of an
 233 experiment, we treated the particle wall-loss corrected aerosol volume concentration $V(t)$
 234 differently before and after its maximum, V_{max} . For

235

$$236 t < t_{V_{max}}, C_{SOA}(t) = (V(t) - V_s)\rho_{SOA},$$

$$237 t \geq t_{V_{max}}, C_{SOA}(t) = [V(t) - V_s \frac{V(t)}{V_{max}}]\rho_{SOA}, \quad (3)$$

238

239 where $t_{V_{max}}$ is the corresponding time at the maximum particle wall-loss corrected total aerosol
 240 volume concentration. V_s is the average particle wall-loss corrected seed volume concentration
 241 before the beginning of each experiment. ρ_{SOA} is the SOA density, assumed to be equal to 1.4 μg
 242 m^{-3} (Kostenidou et al., 2007). Ideally, $V(t)$ should equal to V_{max} after the reactions are completed
 243 and particle wall loss is the only process after $t_{V_{max}}$. However, deviations of $V(t)$ from V_{max} are

244 caused by the uncertainty associated in applying the size-dependent wall-loss corrections. By
245 scaling V_s with $V(t)/V_{\max}$, we are distributing the impact of any potential fluctuations in $V(t)$ evenly
246 to both the seeds and the organics, and thus obtain a more stable C_{SOA} after aging.

247

248 **3.3 Analysis of AMS measurements**

249 The HR-AMS was operated in V mode during the experiments in this work. Squirrel v1.56D was
250 used to analyze the data. The atomic oxygen to carbon ratio, O:C, was determined based on the
251 unit-resolution correlation described in Caragaratna et al. (2015). Nitrate signals were attributed
252 to organics since the only sources of them in these experiments are organonitrates.

253 In an attempt to explore the functionalities/products that may have changed during aging,
254 we used the AMS high-resolution (HR)family analysis. We used Pika 1.15D to analyze the HR
255 data. Each fitted ion is grouped into a “family” based on their chemical formula, and the families
256 used are: CH, CHO, CHO₂, C_x, HO, and NO. These are the main components of the organics
257 formed, with family HO calculated by subtracting the concentrations of the other families from the
258 total organic signal. This is necessary because the fragmentation of sulfates can interfere with the
259 family HO. Family NO can be used to represent the organonitrates formed during the aging phase
260 of the experiments.

261

262 **4. Results and discussion**

263 The particle wall-loss corrected aerosol number concentration evolution during a typical
264 experiment (Exp. 1) together with the SMPS raw measurements are shown in Fig. 1. Prior to the
265 ozonolysis, 18,000 cm⁻³ ammonium sulfate particles were added to the chamber as seeds. After a
266 4.5 h wall-loss period, 8,000 cm⁻³ particles remained suspended, serving as pre-existing surface
267 for condensation. At $t=0$, ozone was added into the chamber, reacting with α -pinene to form
268 condensable first-generation products. The ozonolysis of α -pinene has been found to produce OH
269 with a molar yield of approximately 0.7 (Paulson et al., 1998), which in our experiments resulted
270 in approximately one third of the precursor reacting with OH. An additional 100 cm⁻³ particles
271 were formed due to nucleation at this time. Two doses of HONO were added into the chamber in
272 this experiment at $t=0.4$ h and $t=1.3$ h, respectively. HONO was allowed to mix in the chamber
273 and then the UV lights were turned on at $t=0.8$ h and $t=1.8$ h to produce OH. At $t=3.5$ h, another

274 10,000 cm⁻³ ammonium sulfate particles were added into the chamber for a second 4 h long
275 determination of the $k(D_p)$ profile for this experiment.

276 The two $k(D_p)$ profiles determined from the initial seed wall-loss period and the one at the
277 end of the experiment are shown in Fig. 2. They agree relatively well with small discrepancies at
278 $D_p < 50$ nm. The complete $k(D_p)$ profile used for the size-dependent particle wall-loss correction
279 is also shown.

280 As indicated in Fig. 1, the particle wall-loss corrected aerosol number concentration
281 remains relative level at $t < 0$ h and $t > 3.5$ h, with $\varepsilon_{N,1} = 3.3$ % and $\varepsilon_{N,2} = 0.5$ %, respectively. The
282 particle wall-loss corrected aerosol volume concentration (Fig. 3) at the initial seed wall-loss
283 period and that at the end had variabilities equal to $\varepsilon_{V,initial} = 4.2$ % and $\varepsilon_{V,end} = 3.8$ %,
284 respectively. All parameters were less than 5 % and therefore the accuracy of the wall-loss
285 correction was acceptable.

286 The particle wall-loss corrected aerosol volume concentration evolution for Exp. 1 together
287 with the corresponding SMPS raw measurements are shown in Fig. 3. Particles grew from $t=0$ to
288 0.7 h and $t=0.8$ to 1 h due to vapor condensation. The total aerosol volume peaked at $t=0.7$ h during
289 the first-generation oxidation, and reached its maximum at $t=1.1$ h due to aging during the second-
290 generation oxidation. The change in volume during the second addition of OH at 1.7 h was
291 negligible.

292 The SOA mass concentration evolution for Exp. 1 calculated using Eqn. 3 is shown in Fig.
293 4. The error bars are calculated using the highest ε (in this case $\varepsilon_{V,1} = 4.2$ %). For this experiment,
294 37.7 ± 1.6 $\mu\text{g m}^{-3}$ of SOA was formed during ozonolysis. An additional 11.1 ± 2.6 $\mu\text{g m}^{-3}$ SOA was
295 formed during the first aging period. The SOA reached 48.8 ± 2 $\mu\text{g m}^{-3}$ after aging and remained
296 approximately constant until the end of the experiment. The total SOA produced and the calculated
297 SOA yields for all experiments are listed in Table 2.

298 The AMS-derived atomic oxygen to carbon ratio (O:C) evolution for Exp. 1 is shown
299 together with the AMS-measured aerosol composition (assuming CE=1) in Fig. 5. The increase in
300 the sulfate signals at $t=0$ is caused by a change in the instrument collection efficiency. Due to the
301 uncertainty caused by CE changes over the course of an experiment, we did not use the absolute
302 AMS-measured organic mass concentration for any quantitative analysis. Using the algorithm
303 derived by Kostenidou et al. (2007), we calculated the CE to be ~ 0.25 for the initial seed period
304 and ~ 0.4 after the seeds were coated with organics. A quick check comparing the two stepwise

305 increase in the CE-corrected organic mass concentration to those derived from SMPS revealed that
306 the results from both instrument agreed reasonably well. The algorithm also estimated that the
307 SOA density was $1.3 \pm 0.15 \text{ g cm}^{-3}$ in good agreement with the Kuwata et al. (2012)
308 parameterization based on the measured O:C and H:C which also predicted 1.3 g cm^{-3} .

309 The O:C is a collective measure for the ongoing chemistry during these aging experiments.
310 In Exp. 1, the O:C kept decreasing due to the freshly-formed semi-volatile SOA condensing onto
311 particles from $t=0$ to 0.5 h. Later during the dark period ($t=0.5$ h to 0.8 h), the O:C ratio kept
312 decreasing to 0.42 while the organic mass concentration stayed almost constant. This is consistent
313 with the “ripening” phenomenon, first observed during the MUCHACHAS campaign, where the
314 composition of the formed SOA keeps evolving after α -pinene has reacted while the change in
315 SOA mass is minimal (Tritscher et al., 2011). The nature of this process is not well-understood,
316 but it probably involves heterogeneous reactions. After OH radicals were generated in the chamber
317 at $t=0.8$ h, the semi-volatile vapors got oxidized to form second-generation products of lower
318 volatility, resulting in an increase of 0.02 in O:C in about 10 min. After $t=1$ h, the O:C remained
319 relatively constant but it started to decrease at $t=1.25$ h when the UV lights were turned off. Since
320 aging is a complex process that involves functionalization, fragmentation and heterogeneous
321 reactions, the trends in O:C are indicative of the competition among these processes. The decrease
322 we observed here was associated with turning the UV lights off, and thus it is likely that some
323 chemistry was perturbed and thus the processes resulting in decreasing O:C took over. The
324 decrease in O:C associated with turning off the UV lights was not consistent across the five
325 experiments. This further proves that this phenomenon is the result of several competing process
326 and needs further investigation on a molecular level. An inflection point at $t=1.7$ h was observed
327 after a second dose of OH being introduced in the chamber. Instead of the stepwise increase like
328 the one observed after the first dose of OH, the O:C increased slowly but steadily this time until
329 the end of the experiment to 0.45 with no significant increase in organic mass. This is also quite
330 consistent with what was observed in MUCHACHAS.

331 We used the organic to sulfate ratio (Org/Sulf) derived from AMS measurements to look
332 at the SOA formation in these experiments due to its insensitivity to changes in collection
333 efficiency. The Org/Sulf time series for Exp. 1 is shown in Fig. 6. The ratio increased to 1.25 at
334 $t=0.7$ h as the result of the first-generation vapors condensing onto pre-existing particles. After we
335 first turned on the UV lights, a stepwise increase in the ratio was observed and reached the

336 maximum value of 1.60 at t=1.1 h as a result of the second-generation oxidation chemistry. After
 337 that, the ratio kept decreasing. A small bump was observed after the second introduction of OH
 338 and then the ratio kept decreasing. One possible explanation for this continuous decrease is the
 339 effect of the size-dependent particle wall-loss process. The faster removal of smaller particles
 340 (which contain more SOA than sulfate) than that of the bigger ones (which have a lower SOA to
 341 sulfate ratio) can lead to a decrease of the overall organic to sulfate ratio. Fig. 7 shows the size
 342 dependence of the Org/Sulf, together with the mass distribution of both organic and sulfate for
 343 Exp. 1. The Org/Sulf decreased dramatically from 10 to 1 over the particle vacuum aerodynamic
 344 diameter (D_{va}) range of 200 – 500 nm, indicating strong composition dependence on particle size.
 345 Since the majority of the mass is distributed in this range, the size-dependent particle wall-loss rate
 346 can contribute significantly to the decrease observed in Fig. 6 after the Org/Sulf reached its
 347 maximum.

348

349 **4.1 Effect of size-dependent losses on the organic to sulfate ratio**

350 To quantify the effect of the size-dependence of the particle wall-loss process on the
 351 organic to sulfate ratio, we discretized the AMS-measured mass distribution $M(D_p)$ into 10 bins
 352 in the particle diameter space and defined a mass-weighted particle wall-loss rate constant for each
 353 species j , \bar{k}_j , as

354

$$355 \quad \bar{k}_j = \frac{\sum_{i=1}^{10} M_{ij} k_i}{\sum_{i=1}^{10} M_{ij}} \quad (4)$$

356

357 where M_{ij} is the aerosol mass concentration of species j for size bin i and k_i is the averaged $k(D_p)$
 358 across size bin i . Note that the particle diameter used in this section refers to the SMPS-measured
 359 mobility equivalent diameter D_p . The particle vacuum aerodynamic diameters derived from the
 360 AMS measurements have been converted to D_p using an SOA density of $1.4 \mu\text{g m}^{-3}$.

361 From Eqn. 4 we are able to determine a mass-weighted particle wall-loss rate constant for
 362 sulfate, \bar{k}_{SO_4} , and for organics, \bar{k}_{Org} . For the period after completion of the reactions and if there
 363 are only particle losses to the walls the Org/Sulf ratio should satisfy:

364

$$365 \quad (\text{Org/Sulf})(t) = (\text{Org/Sulf})_m(t) \exp(\bar{k}_{SO_4} - \bar{k}_{Org})t \quad (5)$$

366

367 where $(\text{Org/Sulf})_m(t)$ is the AMS-measured and $(\text{Org/Sulf})(t)$ the loss-corrected organic to
368 sulfate ratio.

369 We can test if indeed the particle wall losses are responsible for the decreasing ratio in Exp.
370 1 focusing on the period from $t_1 = 1.2$ h to $t_2 = 1.7$ h (Fig. 6). In this example t_1 corresponds to
371 the maximum Org/Sulf and t_2 is the second time in which the UV lights were turned on. Applying
372 Eqn. 4, we found the mass-weighted particle wall-loss rate constant for organics, $\bar{k}_{org} = 0.06 \text{ h}^{-1}$,
373 and for sulfate, $\bar{k}_{SO_4} = 0.05 \text{ h}^{-1}$. The black line in the inset graph of Fig. 6 indicates the particle
374 wall-loss corrected Org/Sulf for the chosen time period using Eqn. 5. The loss-corrected ratio
375 remained relatively constant indicating that the size-dependent particle wall-loss process coupled
376 with the different size distributions of the sulfate and organics were causing the decrease in the
377 ratio. This exercise was repeated for the other experiments arriving in the same conclusion.

378

379 4.2 Effect of chemical aging on additional SOA formation

380 To quantify aging effects based on the SMPS measurements, we define the fractional
381 change in the particle wall-loss corrected SOA mass concentration after aging, $\Delta[\text{OA}]$, as:

382

$$383 \Delta[\text{OA}] = (C_{\text{SOA},2} - C_{\text{SOA},\text{UV}}) / C_{\text{SOA},1}, \quad (6)$$

384

385 where $C_{\text{SOA},\text{UV}}$ is the particle wall-loss corrected aerosol mass concentration at the time when we
386 first turned on the UV lights. $C_{\text{SOA},\text{UV}}$ can be equal to $C_{\text{SOA},1}$ depending on how level the first-
387 generation SOA mass concentration remains after wall-loss correction. Fig. 8 summarizes the
388 $\Delta[\text{OA}]$ for all five experiments with the values and corresponding errors listed in Table 2. The OH
389 exposure resulted in an average increase of 24 ± 6 % in SOA mass concentration after aging, ranging
390 from 20 to 29 %. Our HONO injection method creates OH levels of about 2.4×10^7 molecules
391 cm^{-3} for the first hour and then the concentration dropped to around 5×10^6 molecules cm^{-3} . The
392 OH exposure is equivalent to 2-4 days of typical atmospheric oxidation conditions, assuming an
393 OH concentration of 2×10^6 molecules cm^{-3} . The uncertainties displayed in Fig. 8 were propagated
394 from uncertainties in the SOA mass concentration.

395 To quantify aging effects based on the AMS data, we define the fractional change in the
396 organic to sulfate ratio:

397

398
$$\Delta[\text{Org/Sulf}] = ([\text{Org/Sulf}]_2 - [\text{Org/Sulf}]_{\text{UV}}) / [\text{Org/Sulf}]_1, \quad (7)$$

399

400 where $[\text{Org/Sulf}]_{\text{UV}}$ refers to the organic to sulfate ratio at the time when we first turned on the UV
401 lights, $[\text{Org/Sulf}]_1$ the maximum before we first turned on the UV lights and $[\text{Org/Sulf}]_2$ the
402 maximum after the OH exposure. Fig. 8 summarizes the $\Delta[\text{Org/Sulf}]$ calculated for all five
403 experiments with the values and corresponding errors listed in Table 2. The uncertainties are based
404 on the deviation between the measured and the corrected Org/Sulf (Fig. 6 inset) over the chosen
405 time period. An associated error is calculated respectively for $[\text{Org/Sulf}]_{\text{UV}}$, $[\text{Org/Sulf}]_1$ and
406 $[\text{Org/Sulf}]_2$. The reported error for $\Delta[\text{Org/Sulf}]$ in Table 2 is the propagated results of the three.
407 For experiments in this work, the percent increase in organic to sulfate ratios ranged from 18 to
408 27 % with an average increase of 21 ± 4 %. The values are fairly consistent with the SMPS-derived
409 $\Delta[\text{OA}]$.

410

411 **4.2.1 Role of RH**

412 Exp. 5, performed at the intermediate RH of 50 %, resulted in a comparable change in SOA
413 formation after aging as experiments at lower RH (Fig. 8). In this experiment, the increase in
414 Org/Sulf after aging was 21.2 %, 1.5 % higher than the average $\Delta[\text{Org/Sulf}]$ of experiments 2-4.
415 $\Delta[\text{OA}]$ for Exp. 5 was 20.5 %, about 2 % lower than the average $\Delta[\text{OA}]$ of experiments 2-4. The
416 effect of RH on the SOA formation during chemical aging, at least for these conditions, appears
417 to be small.

418

419 **4.2.2 Role of organic vapor loss to the Teflon walls**

420 For chamber SOA experiments with preexisting particles, the particles act as competing
421 surface against the chamber walls. We calculated the condensation sink (CS) of particles using the
422 method described in Trump et al. (2014) with a unit accommodation coefficient, consistent with
423 recent findings (Julin et al., 2014; Palm et al., 2016). The calculated condensation sink in the form
424 of time scale for vapors condensing onto particles ($1/\text{CS}$) for Exp. 1 is shown in Fig. 9. During the
425 entire experiment, the timescale for vapors to condense onto particles remained less than a minute.
426 Compared to the organic vapor wall-loss timescale of 15 min in the CMU chamber (Ye et al.,
427 2016), the vapors condense onto the particles 15 times faster than that onto the walls. This

428 corresponds to a 6.3 % loss of the semi-volatile vapors to the walls. Assuming the yields for the
429 experiments conducted in this work also increase by 6.3 %, the absolute yields should be increased
430 by 1-3 % after accounting for the vapor wall-loss effect. This approach is a conservative estimation
431 of vapor wall loss, and yet the results are consistent with what we observed from the measurements.
432 As indicated in Fig. 6, the organic to sulfate ratio stayed practically constant after its first peak at
433 $t=0.7$ h until the introduction of OH. This is consistent with the fact that the semi-volatiles formed
434 in our system only accounted for a small fraction of the products. Ye et al. (2016) studied the
435 SVOCs formed in the α -pinene ozonolysis system and found 20 % SVOCs in the products formed
436 from experiments with moderate precursor concentration (α -pinene=75 ppb). They also observed
437 that the SVOC fraction increased with increased amounts of reacted α -pinene. Since the reacted
438 α -pinene in our experiments was less than 35 ppb, our observation of small amount of SVOCs
439 forming is also consistent with their results.

440 The situation is a little more complex for the second-generation oxidation because material
441 with higher volatilities that could have become SOA were lost during the time after the end of the
442 first phase and before the beginning of the second. To address this issue, OH radicals were
443 introduced about an hour earlier in Exp. 1 as compared to the rest of the experiments. A shorter
444 timescale ensures the first-generation vapor products react efficiently with OH instead of
445 interacting with the chamber walls as in the case of longer timescales. There was an increase of
446 27 % in Org/Sulf in this experiment after aging, 7 % more than the average of the other four
447 experiments. Δ [OA] for Exp. 1 was 29.4 %, about 7.5 % higher than the average of the rest four
448 experiments. If we attribute this 7 % difference purely to the vapor wall-loss effect, then we
449 estimate that vapor losses can increase the additional SOA formation by roughly another 10 % for
450 the experiments conducted in this work.

451

452 **4.3 Effect of chemical aging on aerosol composition**

453 Fig. 10 summarizes the absolute increase in O:C after the two doses of OH, respectively,
454 with the corresponding exposure required to achieve the increase. As we discussed above using
455 Exp. 1 as an example, the O:C in all experiments showed a stepwise increase after the first OH
456 introduction while it grew continuously after the second OH introduction until the end of the
457 experiment. For these five experiments, it took 10 - 30 min for the O:C to increase by 0.02-0.04.
458 The stepwise increase in O:C is caused by the rapid reactions between the first generation vapor

459 products and the OH. One of the major products identified in the gas phase from the α -pinene
460 ozonolysis system, pinonaldehyde, reacts with OH at a rate of $4.4 \times 10^{-11} \text{ cm}^3 \text{ molecule}^{-1} \text{ s}^{-1}$
461 (Atkinson and Arey, 2003). During the first hour of OH introduction, the OH concentration
462 remains on average at a steady state of $2.4 \times 10^7 \text{ molecule cm}^{-3}$. A quick estimation of
463 $1/k_{OH}[OH]$ gives a timescale of 16 min, which is consistent with what we observed in these
464 experiments.

465 The second exposure corresponds to the period until the end of each experiment. The
466 increase in O:C of 0.01 to 0.04 during this stage clearly indicates change in SOA composition,
467 however paired with minimum change in SOA mass. Although gas-phase reactions can contribute
468 to these observed changes in O:C, the corresponding condensation of the products should also
469 result in a detectable increase in SOA concentration during the same period. Given that changes
470 in SOA concentration could not be detected the contribution of gas-phase oxidation was probably
471 small. In addition, we observed small amounts of SVOCs forming in our system as discussed above.
472 The significant change in O:C without corresponding increase in SOA mass concentration was
473 likely caused by heterogeneous reactions.

474 Based on the HR family analysis results, the less oxidized ion family CH decreased around
475 10 percent during the aging process (i.e., from 41.9 to 38.1 percent of the OA in Exp. 1 and from
476 40.5 to 35.3 percent in Exp. 2) while the more oxidized CHO_2 increased 4 percent in Exp. 1 (from
477 12.8 to 13.3 percent) and 16 percent in Exp. 2 (from 14.9 to 17.3 percent). The changes in the
478 family CHO were +4 percent in Exp. 1 and -6 percent in Exp. 2, suggesting that there was both
479 production and destruction of the corresponding family members. The concentration of
480 organonitrates was, as expected, close to zero initially in these experiments. At the end of the aging
481 process, the NO family represented 3-3.5 % of the OA.

482 CO_2^+ (m/z 44) from family CHO_2 and $\text{C}_2\text{H}_3\text{O}^+$ (m/z 43) from family CHO are usually
483 identified in aged and relatively fresh aerosols, respectively. Their fractions of the total organics,
484 f_{44} and f_{43} , have been used as chemical indicators in chamber experiments (Donahue et al., 2012).
485 During the dark ozonolysis period of Exp. 1 (Fig. S2), the f_{43} increased initially and stayed
486 practically constant after $t=0.2$ h, while f_{44} decreased. After the first introduction of OH, both f_{43}
487 and f_{44} showed a stepwise increase. After the second introduction of OH, f_{43} decreased while f_{44}
488 increased over time until the end of the experiment, indicating that the SOA was getting
489 progressively more oxidized during aging. During Exp. 2 (Fig. S4), f_{43} increased sharply initially

490 and then slowly decreased during the dark ozonolysis period. This is consistent with the “ripening”
491 effect observed during the MUCHACHAS campaign (Donahue et al., 2012). Overall, f_{43}
492 decreased while f_{44} increased over the course of Exp. 2, indicating that the initially formed SOA
493 was getting more oxidized during aging.

494

495 **4.4 Comparison with other studies**

496 Overall, the results from our chamber experiments in this work are consistent to those from
497 the MUCHACHAS chambers. After adopting a size-dependent particle wall-loss correction
498 method, we observed 20-30 % additional SOA formation after aging. Vapor wall-loss effect can
499 account for an additional 10 %, increasing the range to 20-40 %. The O:C presented a stepwise
500 increase of 0.02-0.04 after the first introduction of OH, and then increased gradually overtime after
501 the second introduction of OH.

502 During the MUCHACHAS campaign, mixtures of SOA and gas-phase products formed in
503 the Paul Scherrer Institute (PSI) 27 m³ Teflon chamber from low (10 ppb) and high (40 ppb) initial
504 α -pinene concentration were exposed to OH by TME ozonolysis and HONO photolysis at an RH
505 of approximately 50 % (Tritscher et al. 2011). An OH concentration of 2×10^6 to 10×10^6 molecules
506 cm⁻³ was maintained up to four hours. The authors reported an additional 50 % SOA mass forming
507 after aging using the first-order, size-independent particle wall-loss correction for the suspended
508 organic mass concentration measured by AMS. An increase of 0.04 in the oxygen to carbon ratio
509 was also observed during aging.

510 In the 84.5 m³ Aerosol Interaction and Dynamics in the Atmosphere (AIDA) aluminum
511 chamber at Karlsruhe Institute of Technology, an OH concentration of 2×10^6 to 10×10^6 molecules
512 cm⁻³ was used by a constant flow of TME (dark aging). The authors observed an increase of 17-
513 55 % in the SMPS-derived SOA mass concentration (density corrected) after aging during four
514 experiments with initial α -pinene concentration ranging from 14 to 56 ppb (Salo et al., 2011). In
515 the 270 m³ Simulation of Atmospheric Photochemistry in a large Reaction (SAPHIR) Teflon
516 chamber at Forschungszentrum Jülich, SOA and vapors generated from the ozonolysis of 40 ppb α -
517 pinene was aged for three consecutive days with OH produced by ambient light chemistry. An OH
518 concentration of $2-5 \times 10^6$ molecules cm⁻³ was maintained and 9 %, 4 % and 1 % additional SOA
519 was formed respectively after aging each day. These values were corrected for particle wall loss
520 using different wall-loss rate constants determined during different periods of the experiment.

521 Our result of 20-40 % additional SOA formation due to aging is well within the range of
522 that from the above chambers. The difference in the results from each chamber could potentially
523 be attributed to different OH exposure (e.g. a constant flow of HONO or TME was provided in the
524 PSI chamber). Other plausible explanations include whether the reported values were particle wall-
525 loss corrected and whether the same method was adopted for the correction.

526 For the HONO aging experiment performed in the CMU chamber during the
527 MUCHACHAS campaign, Henry and Donahue (2012) suggested a potentially strong photolysis
528 effect based on decreasing organic to sulfate ratio derived from the AMS measurements. In our
529 experiments, the organic to sulfate ratio was affected by the size-dependent wall-loss process. Both
530 the AMS-measured organic to sulfate ratio and the SMPS-measured OA remained relatively
531 constant after correcting for the size dependence of the particle-wall process in these experiments.
532 We thus conclude that minimum photolysis was observed for our experiments.

533

534 **5. Conclusions**

535 With an OH exposure equivalent to 2-4 days of typical atmospheric oxidation conditions,
536 the OH aging of the α -pinene ozonolysis products formed 20-40 % additional SOA mass for the
537 experimental conditions used in this work. Elevated RH up to 50 % has minimum effect on SOA
538 production due to aging. We have constrained the aging effects on additional SOA formation
539 quantitatively using both SMPS and AMS measurements.

540 A more oxygenated product distribution was observed after aging. A stepwise increase of
541 0.02-0.04 in O:C was observed within half an hour after the first introduction of OH. After the
542 second-generation products were exposed to additional OH, the O:C grew continuously until the
543 end of the experiments with an absolute increase of up to 0.04. During this period, minimum SOA
544 production was observed. We attribute this phenomenon to condensed-phase reactions. Further
545 investigation on a molecular scale is needed.

546 This work explored the additional SOA formation potential of the α -pinene ozonolysis
547 products under high NO_x conditions. The aging time scale of this study of a few days corresponds
548 to the atmospheric lifetime of the corresponding aerosol. The additional formation of SOA
549 observed here is clearly non-negligible, but is also much less than the doubling or tripling of the
550 SOA that has been assumed in few modeling studies (Lane et al., 2008) which resulted in

551 overprediction of the biogenic SOA. The present results can be used for the improvements of the
552 currently used parameterizations for the aging of α -pinene SOA products in CTMs.

553

554 *Acknowledgement:* The work was funded by the EPA STAR grant 835405 and the EUROCHAMP-
555 2020 EU project.

556

557 6. References

558 Atkinson, R., and Arey J.: Atmospheric degradation of volatile organic compounds, *Chemical*
559 *Reviews*, 103, 4605-4638, 2003.

560 Barnet, P., Dommen, J., DeCarlo, P. F., Tritscher, T., Praplan, A. P., Platt, S. M., Prévôt A. S.
561 H., Donahue, N. M., and Baltensperger, U.: OH clock determination by proton transfer
562 reaction mass spectrometry at an environmental chamber, *Atmos. Meas. Tech.*, 5, 647–656,
563 2012.

564 Canagaratna, M. R., Jimenez, J. L., Kroll, J. H., Chen, Q., Kessler, S. H., Massoli, P., Hildebrandt
565 Ruiz, L., Fortner, E., Williams, L. R., Wilson, K. R., Surratt, J. D., Donahue, N. M., Jayne,
566 J. T., and Worsnop, D. R.: Elemental ratio measurements of organic compounds using
567 aerosol mass spectrometry: characterization, improved calibration, and implications,
568 *Atmos. Chem. Phys.*, 15, 253-272, 2015.

569 Chacon-Madrid, H. J., Henry, K. M., and Donahue, N. M.: Photo-oxidation of pinonaldehyde at
570 low NO_x: from chemistry to organic aerosol formation, *Atmos. Chem. Phys.*, 13, 3227-
571 3236, 2013.

572 Cocker III, D. R., Flagan, R. C., and Seinfeld, J. H.: State-of-the-art chamber facility for studying
573 atmospheric aerosol chemistry, *Environ. Sci. Technol.*, 35, 2594–2601, 2001.

574 Crump, J. G., and Seinfeld, J. H.: Turbulent deposition and gravitational sedimentation of an
575 aerosol in a vessel of arbitrary shape, *J. Aerosol Sci.*, 2, 405–415, 1981.

576 Davidson, C. I., Phalen, R. F., and Solomon, P. A.: Airborne particulate matter and human health:
577 a review, *Aerosol Science and Technology*, 39, 737–749, 2005.

578 Donahue, N. M., Henry, K. M., Mentel, T. F., Kiendler-Scharr, A., Spindler, C., Bohn, B., Brauers,
579 T., Dorn, H. P., Fuchs, H., Tillmann, R., Wahner, A., Saathoff, H., Naumann, K.-H.,
580 Mohler, O., Leisner, T., Müller, L., Reinnig, M.-C., Hoffmann, T., Salo, K., Hallquist, M.,
581 Frosch, M., Bilde, M., Tritscher, T., Barnet, P., Praplan, A. P., DeCarlo, P. F., Dommen,
582 J., Prevot, A. S. H., and Baltensperger, U.: Aging of biogenic secondary organic aerosol
583 via gas-phase OH radical reactions, *Proc. Natl. Acad. Sci., U.S.A.*, 109, 13503 –13508,
584 2012.

585 Donahue, N. M., Robinson, A. L., Stanier, C. O., and Pandis, S. N.: Coupled partitioning, dilution
586 and chemical aging of semivolatile organics, *Environ. Sci. Technol.*, 40, 2635-2643, 2006.

587 George, I. J., Slowik J., and Abbatt J. P. D.: Chemical aging of ambient organic aerosol from
588 heterogeneous reaction with hydroxyl radicals, *Geophys. Res. Lett.*, 35, L13811, 2008.

589 Griffin, R. J., Cocker, D. R., Seinfeld, J. H., and Dabdub, D.: Estimate of global atmospheric
590 organic aerosol from oxidation of biogenic hydrocarbons, *Geophys. Res. Lett.*, 26, 2721–
591 2724, 1999.

592 Henry, K. M., and Donahue, N. M.: Photochemical aging of α -pinene secondary organic aerosol:
593 effects of OH radical sources and photolysis: *J. Phys. Chem. A*, 116, 5932–5940, 2012.

594 Henry, K. M., Lohaus T., and Donahue, N. M.: Organic aerosol yields from α -pinene oxidation:
595 bridging the gap between first-generation yields and aging chemistry, *Environ. Sci.*
596 *Technol.*, 46, 12347–12354, 2012.

597 Intergovernmental Panel on Climate Change: Climate Change 2007: Synthesis Report.
598 Contribution of Working Groups I, II and III to the Fourth Assessment Report of the
599 Intergovernmental Panel on Climate Change, edited by R. K. Pachauri and A. Reisinger,
600 eds., 104 pp., Cambridge Univ. Press, New York, 2007.

601 Julin, J., Winkler, P. M., Donahue, N. M., Wagner, P. E., and Riipinen, I.: Near-unity mass
602 accommodation coefficient of organic molecules of varying structure, *Environ. Sci.*
603 *Technol.*, 48, 12083–12089, 2014.

604 Kalberer, M., Sax, M., and Samburova, V.: Molecular size evolution of oligomers in organic
605 aerosols collected in urban atmospheres and generated in a smog chamber, *Environ. Sci.*
606 *Technol.*, 40, 5917–5922, 2006.

607 Keywood, M. D., Varutbangkul, V., Bahreini, R., Flagan, R. C., and Seinfeld, J. H.: Secondary
608 organic aerosol formation from the ozonolysis of cycloalkenes and related compounds,
609 *Environ. Sci. Technol.*, 38, 4157–4164, 2004.

610 Krechmer, J. E., Pagonis, D., Ziemann, P. J., and Jimenez, J. L.: Quantification of gas-wall
611 partitioning in Teflon environmental chambers using rapid bursts of low-volatility oxidized
612 species generated in situ, *Environ. Sci. Technol.*, 50, 5757–5765, 2016.

613 Kostenidou E., Pathak R. K., and Pandis S. N.: An algorithm for the calculation of secondary
614 organic aerosol density combining AMS and SMPS data; *Aerosol Science and Technology*,
615 41, 1002–1010, 2007.

616 Kuwata, M., Zorn S. R., and Martin S. T.: Using elemental ratios to predict the density of organic
617 material composed of carbon, hydrogen, and oxygen, *Environ. Sci. Technol.*, 46, 787-794,
618 2012. Lambe, A. T., Miracolo, M. A., Hennigan, C. J., Robinson, A. L., and Donahue, N.
619 M.: Effective rate constants and uptake coefficients for the reactions of organic molecular
620 markers (n-alkanes, hopanes and steranes) in motor oil and diesel primary organic aerosols
621 with hydroxyl radicals, *Environ. Sci. Technol.*, 43, 8794–8800, 2009.

622 Lane, T., Donahue, N. M., and Pandis, S. N.: Simulating secondary organic aerosol formation
623 using the volatility basis-set approach in a chemical transport model, *Atmospheric*
624 *Environment*, 42, 7439-7451, 2008.

625 Loza, C. L., Chhabra, P. S., Yee, L. D., Craven, J. S., Flagan, R. C., and Seinfeld, J. H.: Chemical
626 aging of m-xylene secondary organic aerosol: laboratory chamber study, *Atmos. Chem.*
627 *Phys.*, 12, 151–167, 2012.

628 Matsunaga, A., and Ziemann, P. J.: Gas-wall partitioning of organic compounds in a Teflon film
629 chamber and potential effects on reaction product and aerosol yield measurements, *Aerosol*
630 *Science and Technology*, 44, 881–892, 2010.

631 McMurry, P. H., and Rader, D. J.: Aerosol wall losses in electrically charged chambers, *Atmos.*
632 *Chem. Phys.*, 4, 249–268, 1985.

633 Müller, L., Reinnig, M. C., Naumann, K. H., Saathoff, H., Mentel, T. F., Donahue, N. M., and
634 Hoffmann, T.: Formation of 3-methyl-1,2,3-butanetricarboxylic acid via gas phase
635 oxidation of pinonic acid - a mass spectrometric study of SOA aging, *Atmos. Chem. Phys.*,
636 12, 1483–1496, 2012.

637 Nah, T., McVay, R. C., Zhang, X., Boyd, C. M., Seinfeld, J. H., and Ng, N. L.: Influence of seed
638 aerosol surface area and oxidation rate on vapor wall deposition and SOA mass yields: a
639 case study with α -pinene ozonolysis, *Atmos. Chem. Phys.*, 16, 9361–9379, 2016.

640 Ng, N. L., Kroll, J. H., Chan, A. W. H., Chhabra, P. S., Flagan, R. C., and Seinfeld, J. H.: Secondary
641 organic aerosol formation from m-xylene, toluene, and benzene, *Atmos. Chem. Phys.*, 7,
642 3909–3922, 2007.

643 Palm, B. B., Campuzano-Jost, P., Ortega, A. M., Day, D. A., Kaser, L., Jud, W., Karl, T., Hansel,
644 A., Hunter, J. F., Cross, E. S., Kroll, J. H., Peng, Z., Brune, W. H., and Jimenez, J. L.: In
645 situ secondary organic aerosol formation from ambient pine forest air using an oxidation
646 flow reactor, *Atmos. Chem. Phys.*, 16, 2943–2970, 2016.

647 Paulson, S. E., Chung, M., Sen, A. D., and Orzechowska, G.: Measurement of OH radical
648 formation from the reaction of ozone with several biogenic alkenes, *J. Geophys. Res.*, 103,
649 25533–25539, 1998. Pope, C. A., Ezzati, M., and Dockery, D. W.: Fine-particulate air
650 pollution and life expectancy in the United States, *New Engl. J. Med.*, 360, 376–386, 2009.

651 Qi, L., Nakao, S., and Cocker, D. R.: Aging of secondary organic aerosol from α -pinene ozonolysis:
652 Roles of hydroxyl and nitrate radicals, *Journal of the Air & Waste Management*
653 *Association*, 62, 1359–1369, 2012.

654 Robinson, A. L., Donahue, N. M., Shrivastava, M. K., Weitkamp, E. A., Sage, A. M., Grieshop,
655 A. P., Lane, T. E., Pierce, J. R., and Pandis, S. N.: Rethinking organic aerosol: semivolatile
656 emissions and photochemical aging, *Science*, 315, 1259–1262, 2007.

657 Salo, K., Hallquist, M., Jonsson, Å. M., Saathoff, H., Naumann, K.-H., Spindler, C., Tillmann R.,
658 Fuchs, H., Bohn, B.; Rubach, F., Mentel, T. F., Müller, L., Reinnig, M., Hoffmann, T., and
659 Donahue, N. M.: Volatility of secondary organic aerosol during OH radical induced ageing;
660 *Atmos. Chem. Phys.*, 11, 11055–11067, 2011.

661 Tritscher, T., Dommen, J., DeCarlo, P. F., Gysel, M., Barmet, P. B., Praplan, A. P., Weingartner
662 E., Prévôt, A. S. H., Riipinen, I., Donahue, N. M., and Baltensperger, U.: Volatility and
663 hygroscopicity of aging secondary organic aerosol in a smog chamber, *Atmos. Chem.*
664 *Phys.*, 11, 11477–11496, 2011.

665 Trump, E. R., Riipinen, I., and Donahue, N. M.; Interactions between atmospheric ultrafine
666 particles and secondary organic aerosol mass: a model study, *Boreal Environ. Res.*, 19,
667 352–362, 2014

668 Tsimpidi, A. P., Karydis, V. A., Zavala, M., Lei, W., Bei, N., Molina, L., and Pandis, S. N.: Sources
669 and production of organic aerosol in Mexico City: insights from the combination of a
670 chemical transport model (PMCAMx-2008) and measurements during MILAGRO, *Atmos.*
671 *Chem. Phys.*, 11, 5153–5168, 2011.

672 Wang, N., Donahue, N. M., and Pandis, S.N.: Performance of different particle wall-loss correction
673 methods for aging experiments of alpha-pinene SOA in a smog chamber, *Aerosol Science*
674 *and Technology*; in preparation.

675 Ye, P., Ding, X., Hakala, J., Hofbauer, V., Robinson, E. S., and Donahue, N. M.: Vapor wall loss
676 of semi-volatile organic compounds in a Teflon chamber, *Aerosol Science and Technology*,
677 50, 822–834, 2016.

678 Ye, P., Ding, X., Ye, Q., and Robinson, E. S.: Uptake of semivolatile secondary organic aerosol
679 formed from α -pinene into nonvolatile polyethylene glycol probe particles, *J. Phys. Chem.*
680 *A*, 120, 1459–1467, 2016.

681 Zhang, Q., Jimenez, J. L., Canagaratna, M. R., Allan, J. D., Coe, H., Ulbrich, I., Alfarra, M. R.,
682 Takami, A., Middlebrook, A. M., Sun, Y. L., Dzepina, K., Dunlea, E., Docherty, K., De-

683 Carlo, P. F., Salcedo, D., Onasch, T., Jayne, J. T., Miyoshi, T., Shimono, A., Hatakeyama,
684 S., Takegawa, N., Kondo, Y., Schneider, J., Drewnick, F., Borrmann, S., Weimer, S.,
685 Demerjian, K., Williams, P., Bower, K., Bahreini, R., Cottrell, L., Griffin, R. J., Rautiainen,
686 J., Sun, J. Y., Zhang, Y. M., and Worsnop, D. R.: Ubiquity and dominance of oxygenated
687 species in organic aerosols in anthropogenically-influenced Northern Hemisphere
688 midlatitudes, *Geophys. Res. Lett.*, 34, L13801, 2007.

689 Zhang, X., Cappa, D. C., Jathar, S. H., McVay, R. C., Ensberg, J. J., Kleeman, M. J., and Seinfeld,
690 J. H.: Influence of vapor wall loss in laboratory chambers on yields of secondary organic
691 aerosol, *PNAS*, 111, 5802-5807, 2014.

692

693

694

695

696

697

698

699

700

701

Table 1: Initial conditions of the α -pinene ozonolysis aging experiments.

Experiment	α-pinene (ppb)	O₃ (ppb)	Initial seed surface area ($\mu\text{m}^2 \text{cm}^{-3}$)	RH (%)	OH^a ($\times 10^7$ molecules cm^{-3})	OH introduction time (h after α- pinene consumption)
1	33	450	850	<20	2.4	0.3
2	14	600	760	<20	2.7	0.8
3	35	450	720	<20	2.0	1.1
4	16	500	950	<20	2.4 ^b	1.1
5	20	400	710	~50	2.7	0.8

702

703 ^aThe OH concentration was calculated using the decay of butanol-d9 (monitored by PTRMS)
704 (Barnet et al., 2012).

705 ^bEstimated OH concentration for Exp. 4 based on the other experiments. The PTRMS data was
706 not available during that time for Exp. 4.

707

708

709

710

711

712

713

714

715

716

717

718

719

720

721

722

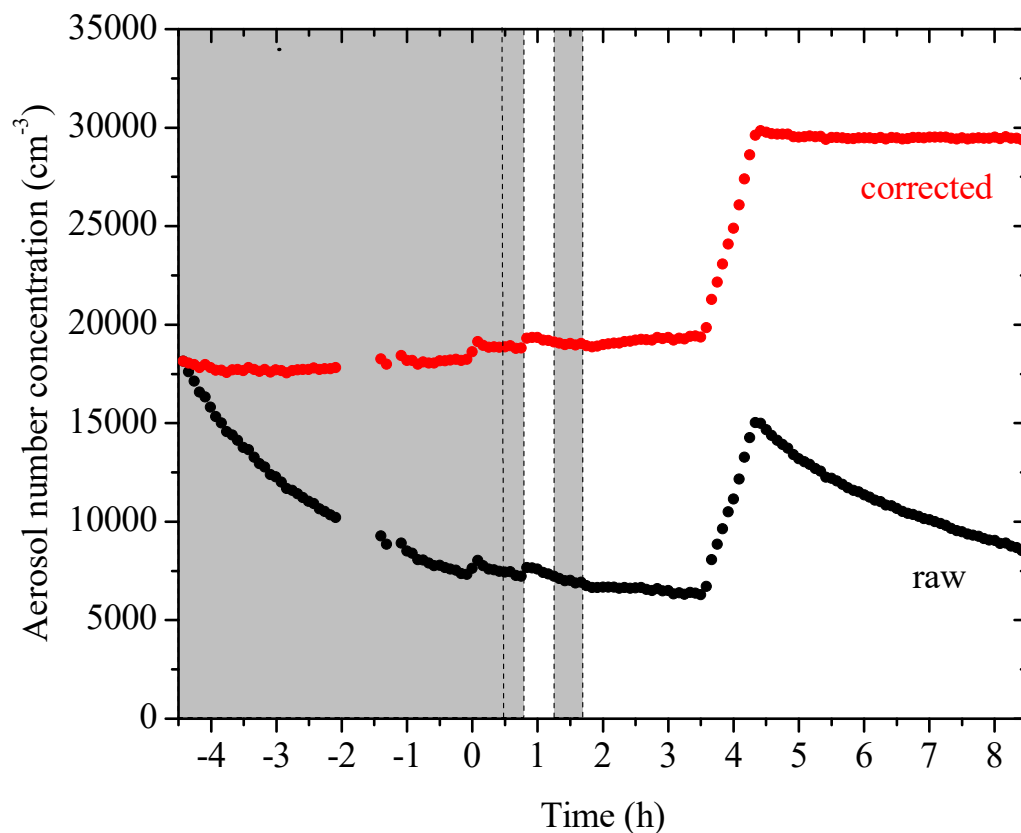
723

724
725
726
727

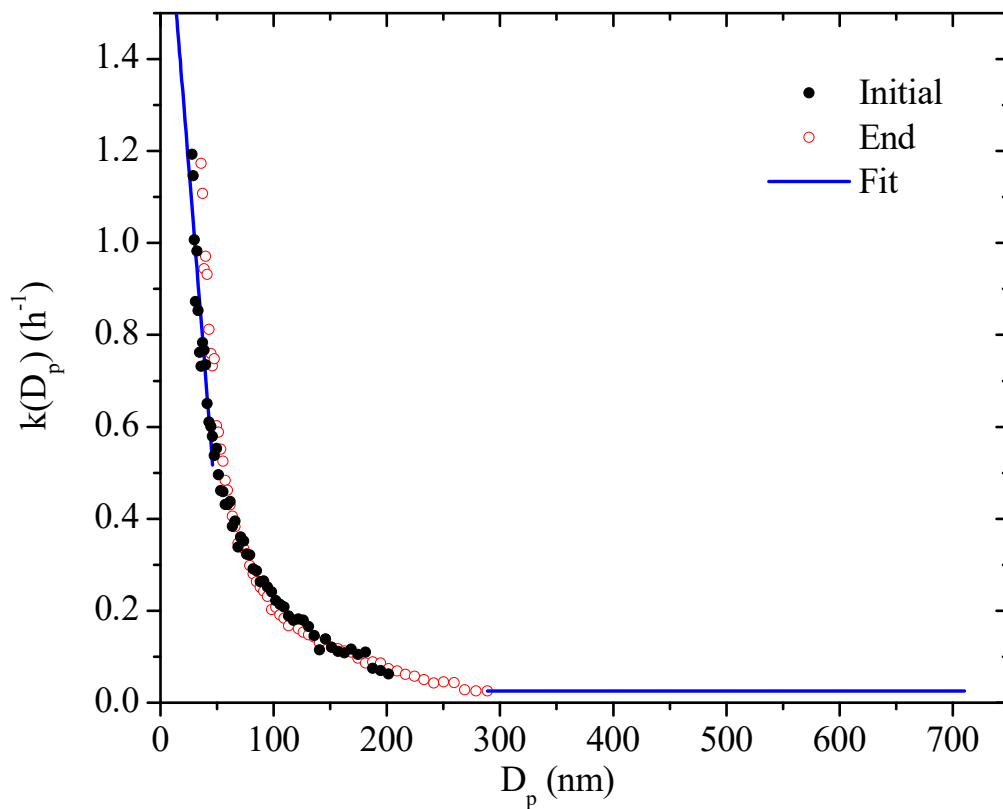
Table 2: SOA mass concentration and yields of the α -pinene ozonolysis aging experiments.

Experiment	$C_{\text{SOA},1}$ ($\mu\text{g m}^{-3}$)	Y_1 (%)	$C_{\text{SOA},2}$ ($\mu\text{g m}^{-3}$)	Y_2 (%)	ΔOA (%)	$\Delta[\text{Org/Sulf}]$ (%)
1	37.7 \pm 1.6	20.6 \pm 0.9	48.8 \pm 2.0	26.7 \pm 1.1	29.4 \pm 6.9	27.0 \pm 5.8
2	16.7 \pm 0.9	21.5 \pm 1.2	18.3 \pm 1.0	23.5 \pm 1.3	19.8 \pm 8.1	18.1 \pm 2.9
3	57.1 \pm 1.3	29.4 \pm 0.7	71.0 \pm 1.6	36.2 \pm 0.8	23.5 \pm 3.6	19.1 \pm 3.6
4	16.8 \pm 0.6	19.1 \pm 0.6	20.8 \pm 0.7	23.7 \pm 0.8	24.0 \pm 5.3	21.9 \pm 2.1
5	22.2 \pm 0.7	19.5 \pm 0.6	25.4 \pm 0.8	22.3 \pm 0.7	20.5 \pm 4.7	21.2 \pm 4.4

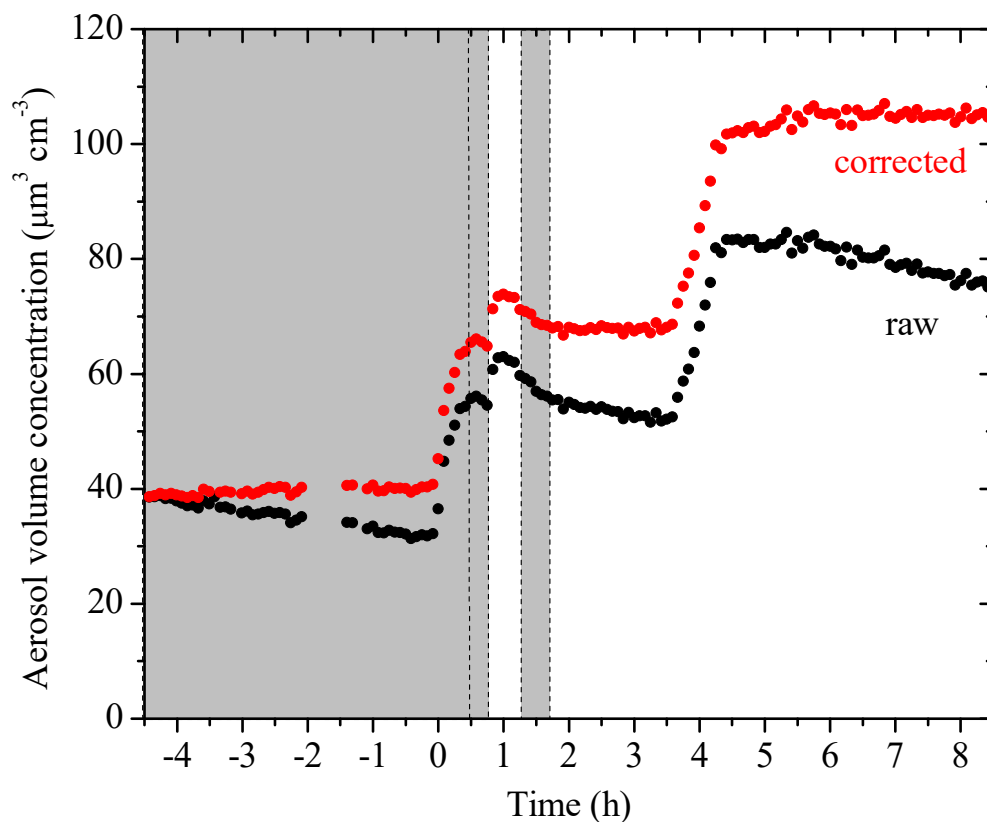
728
729
730
731
732
733
734



735
 736 **Figure 1:** SMPS-measured (black symbols) and the size-dependent particle wall-loss corrected
 737 (red symbols) aerosol number concentration evolution during a typical experiment (Exp. 1). Ozone
 738 was added into the chamber at time zero to initiate α -pinene ozonolysis. The shaded areas indicate
 739 that the chamber was dark. The dashed lines mark the beginning and the end of the two times
 740 HONO were added, respectively. The increase in number concentration at $t=3.5$ h is due to the
 741 injection of 5 g L^{-1} ammonium sulfate particles. An additional 100 cm^{-3} particles were formed due
 742 to nucleation both at the ozonolysis step and the aging step. Data were not recorded from $t=-2$ h to
 743 -1.4 h.
 744
 745
 746



747
 748 **Figure 2:** The size-dependent particle wall-loss rate constant profile, $k(D_p)$, for Exp. 1. The black
 749 symbols are the rate constants calculated based on the wall-loss process of the initial ammonium
 750 sulfate seed particles from $t=-4.5$ h to $t=0$ h, while the red open symbols those of the additional
 751 ammonium sulfate particles at the end from $t=4.5$ h to $t=8.5$ h. The blue line is the fit determined.
 752
 753
 754
 755

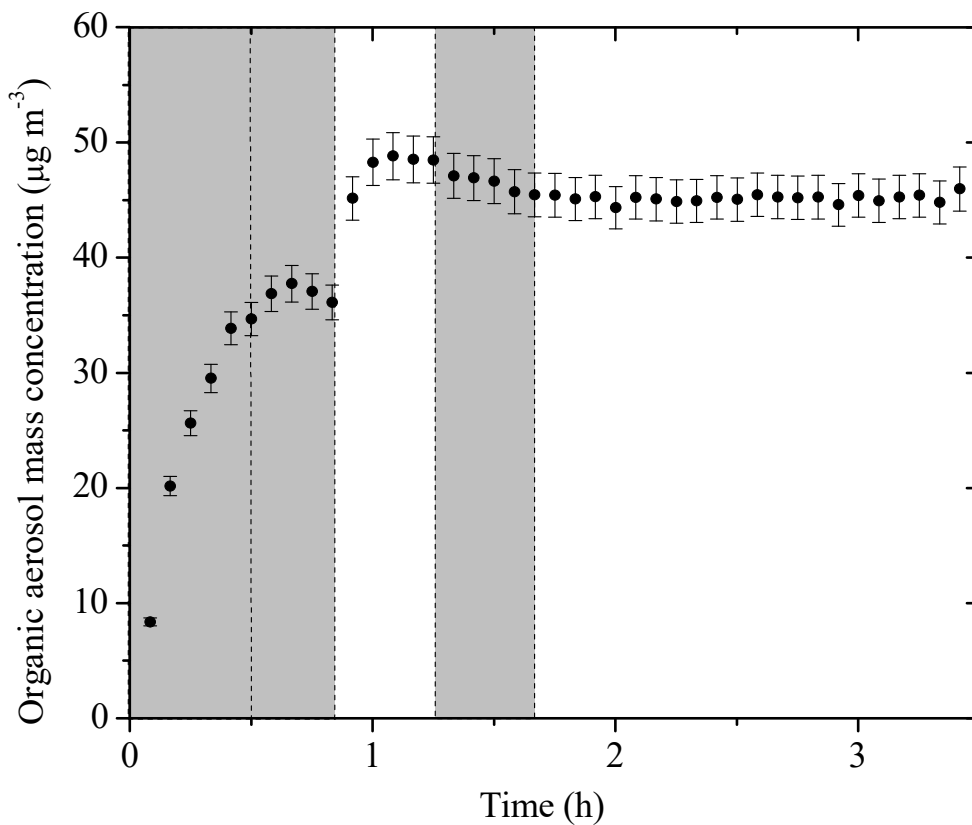


756

757 **Figure 3:** SMPS-measured (black symbols) and the size-dependent particle wall-loss corrected
 758 (red symbols) aerosol (seed and organic) volume concentration evolution during a typical
 759 experiment (Exp. 1). Ozone was added into the chamber at time zero to initiate α -pinene ozonolysis.
 760 The shaded areas indicate that the chamber was dark. The dashed lines mark the beginning and the
 761 end of the two times HONO were added, respectively. 5 g L^{-1} ammonium sulfate particles were
 762 injected into the chamber at $t=3.5 \text{ h}$. Data were not recorded from $t=-2 \text{ h}$ to -1.4 h .

763

764



765
 766
 767 **Figure 4:** The particle wall-loss corrected SOA mass concentration ($\rho=1.4 \text{ g cm}^{-3}$) evolution for
 768 Exp. 1 derived from SMPS measurements. The corresponding error shown is due to the particle
 769 wall-loss correction. Ozone was added into the chamber at time zero to initiate α -pinene ozonolysis.
 770 The shaded areas indicate that the chamber was dark. The dashed lines mark the beginning and the
 771 end of the two times HONO were added, respectively.

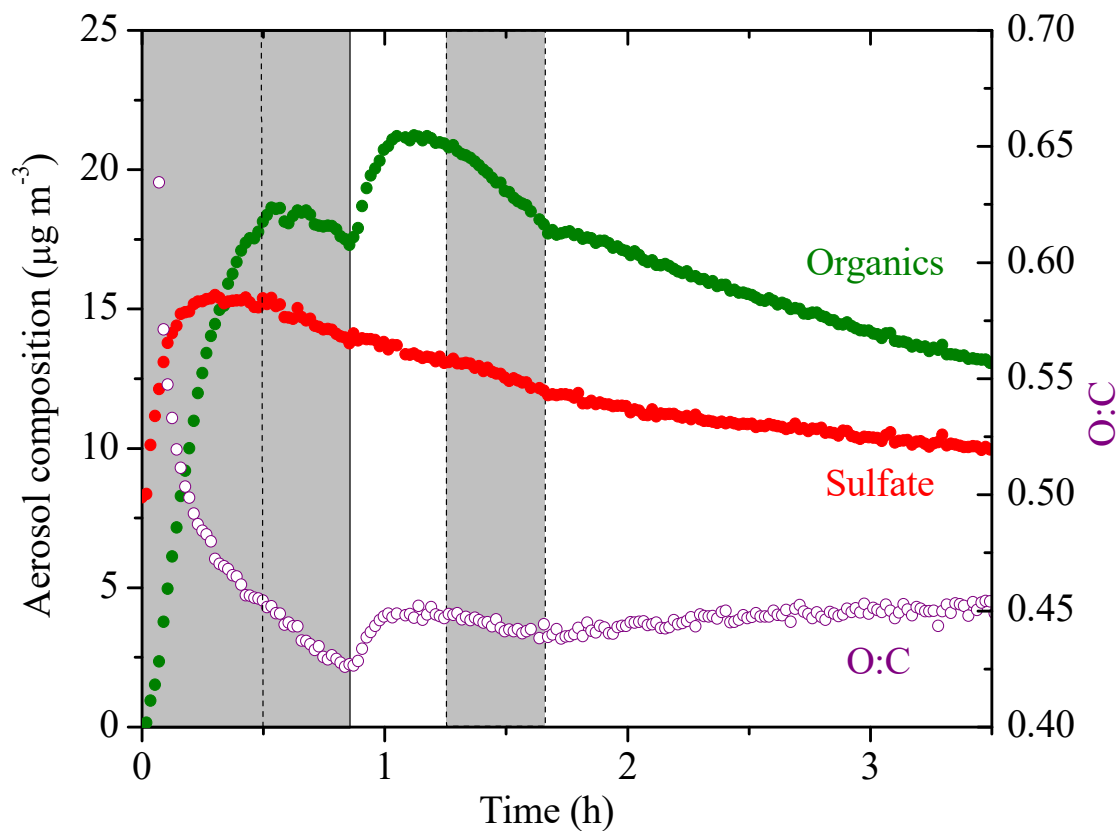
772

773

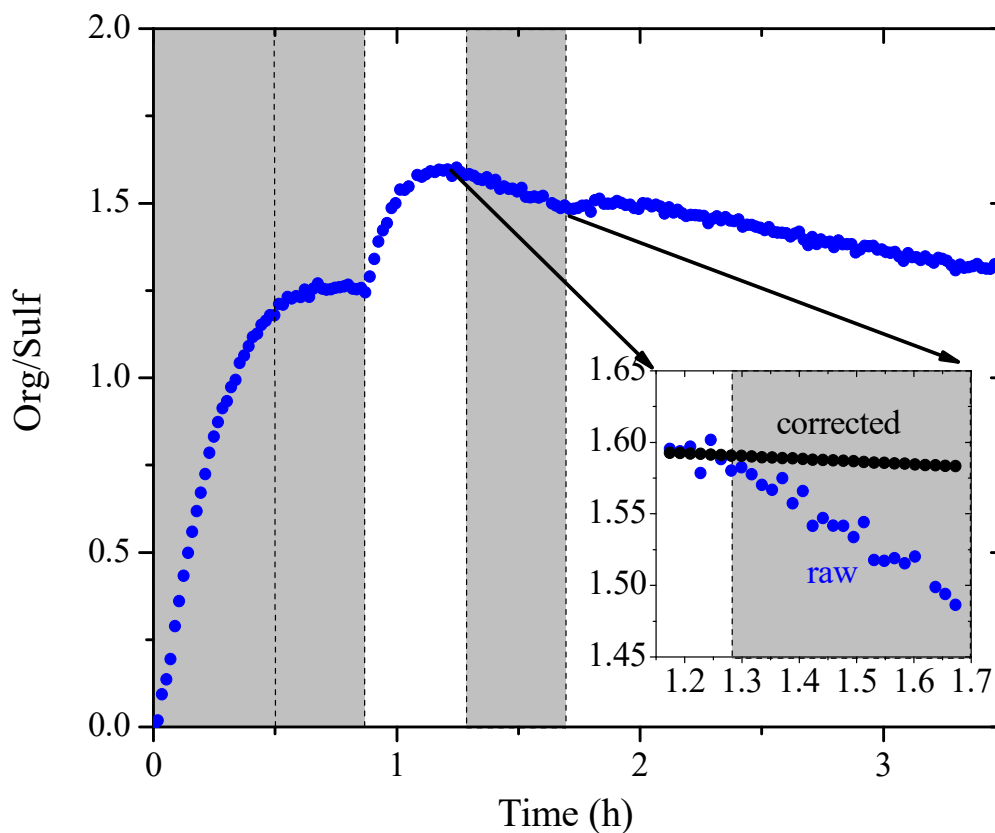
774

775

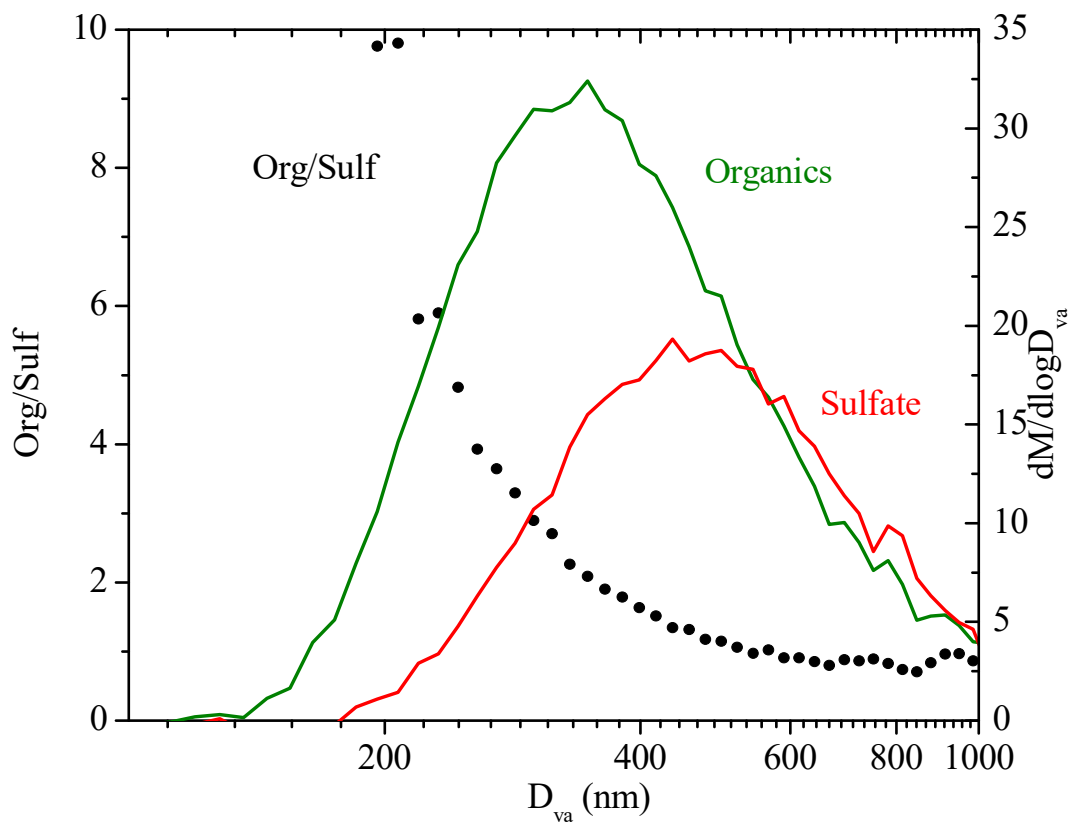
776



777
 778 **Figure 5:** The AMS-measured aerosol composition (CE=1) (left axis) and the atomic oxygen to
 779 carbon ratio (right axis) evolving with time for Exp. 4. The increase in the sulfate signal at $t=0$ is
 780 the result of a change in the collection efficiency (CE). Ozone was added into the chamber at time
 781 zero to initiate α -pinene ozonolysis. The shaded areas indicate that the chamber was dark. The
 782 dashed lines mark the beginning and the end of the two times HONO were added, respectively.



783
 784 **Figure 6:** The AMS-derived organic to sulfate ratio time series for Exp. 1. The inset is a blow-up
 785 of the Org/Sulf ratio from its maximum until the second time when the UV lights were turned on.
 786 The black symbols are the particle wall-loss corrected Org/Sulf during that half hour. Ozone was
 787 added into the chamber at time zero to initiate α -pinene ozonolysis. The shaded areas indicate that
 788 the chamber was dark. The dashed lines mark the beginning and the end of the two times HONO
 789 were added, respectively.



790

791 **Figure 7:** The dependence of the AMS-derived organic to sulfate ratio on particle vacuum
 792 aerodynamic diameter for Exp. 1 (left axis). Also shown are the AMS-measured organic (green)
 793 and sulfate (red) mass distribution (right axis). The results are based on PToF data averaged over
 794 ~2.5 hours ($t=1.1$ h to 3.5 h).

795

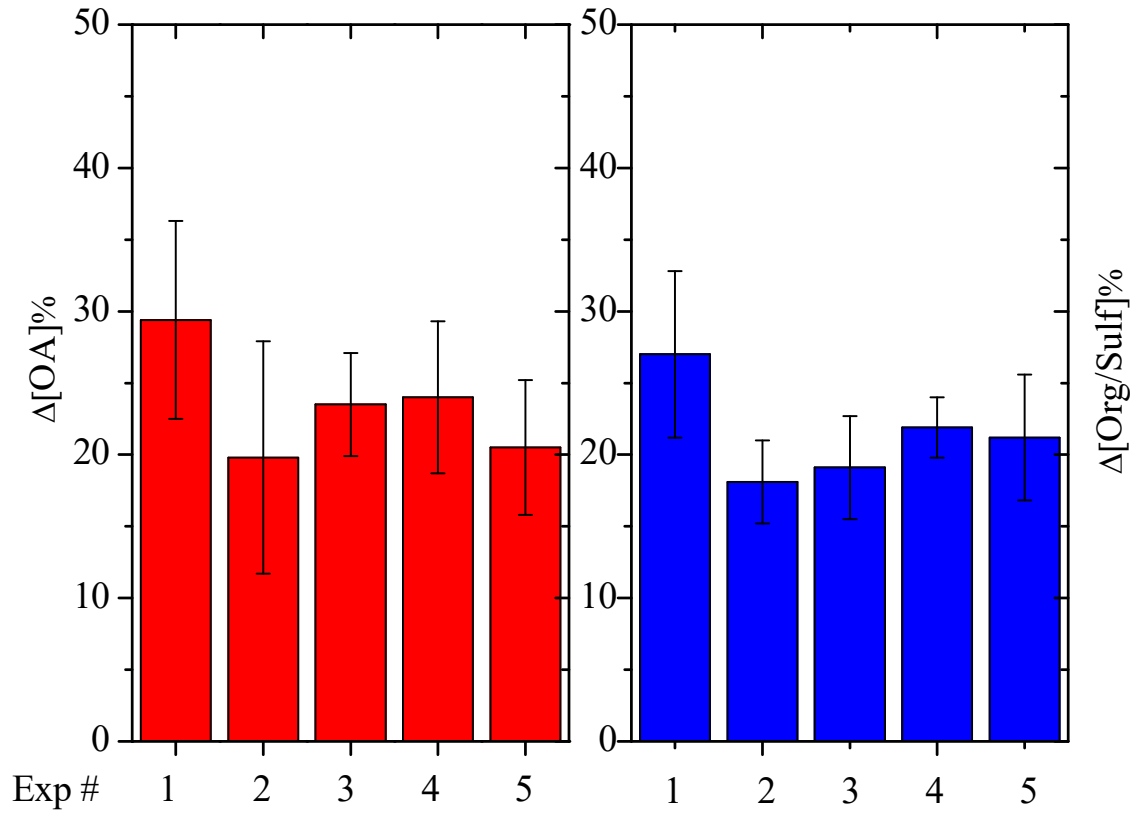
796

797

798

799

800



801

802

803 **Figure 8:** SMPS-derived percent change in the particle wall-loss corrected SOA (red columns)
 804 mass concentration after aging and AMS-derived percent change in organic to sulfate ratio (blue
 805 columns) after aging for all five experiments.

806

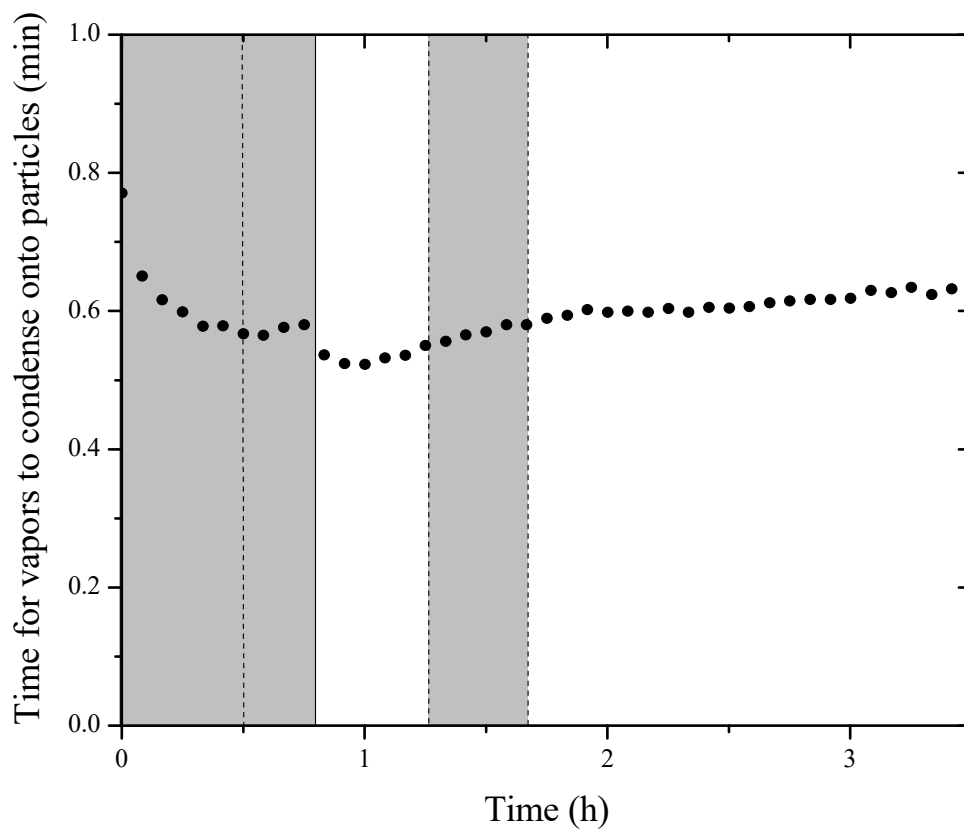
807

808

809

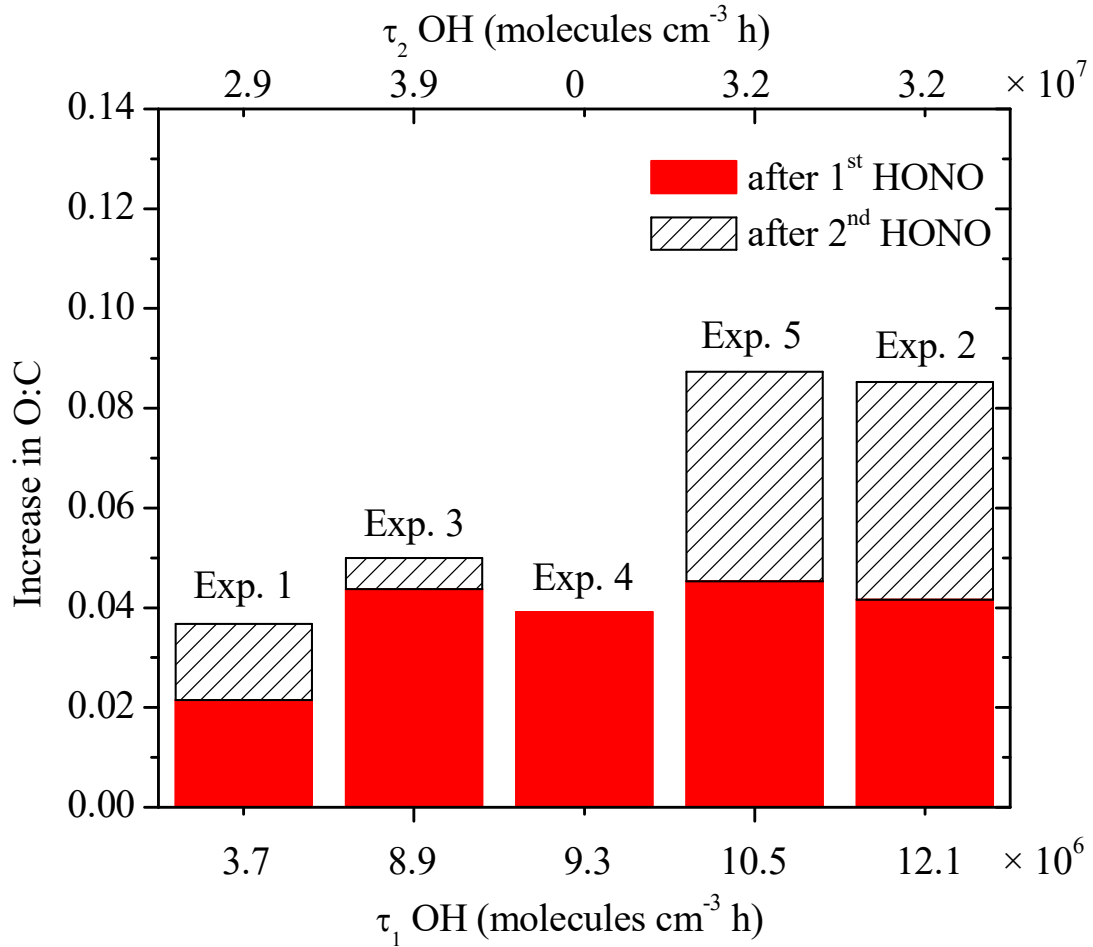
810

811



812

813 **Figure 9:** The calculated condensation sink (CS) in the form of time scale for vapors condensing
 814 onto particles (1/CS). Ozone was added into the chamber at time zero to initiate α -pinene
 815 ozonolysis. The shaded areas indicate that the chamber was dark. The dashed lines mark the
 816 beginning and the end of the two times HONO were added, respectively.



817

818

819 **Figure 10:** The absolute increase in O:C after the two doses of OH, respectively, with the
 820 corresponding exposure. The solid red columns are the increase in O:C after the first introduction
 821 of OH, with the corresponding exposure on the bottom axis. The hatched columns are the increase
 822 in O:C after the second introduction of OH, with the corresponding exposure on the top axis.

823

824

825

826

827

828

829